# *In vivo* isogenic modelling unveils a *TP53*-mediated relapse phenotype in T-cell acute lymphoblastic leukemia

Stéphanie Gachet[1,2,3,#], Samuel Quentin[1,2,4*], Lucie Hernandez[1,2*], Loïc Maillard[1,2], Marie Passet[1,2,4], Rathana Kim[1,2,3,4], Hugo Bergugnat[1,2], Melha Benlebna[1,2], Maxime Boy[1,2], Véronique Parietti[1,2], Pierre Fenaux[5], André Baruchel[6], Hervé Dombret[1,4,5], Nicolas Boissel[1,2,3,7], François Sigaux[1,2,3,4], Hugues de Thé[1,2,3,4], Emmanuelle Clappier[1,2,3,4] and Jean Soulier[1,2,3,4].

[1]Institut de Recherche Saint-Louis (IRSL), Université Paris Cité, 75010 Paris, France;
[2]INSERM UMR1342 / CNRS EMR8000, Paris, France;
[3]Institut de la Leucémie, Hôpital Saint-Louis, APHP, Université Paris Cité, Paris, France;
[4]Hôpital Saint-Louis, Laboratoire d'Hématologie, APHP, Paris, France;
[5]Hôpital Saint-Louis, Département Hématologie Senior, APHP, Paris, France;
[6]Hôpital Robert Debré, APHP, Université Paris Cité, Paris, France;
[7]Hôpital Saint-Louis, Service d'Hématologie Adolescents et Jeunes Adultes, APHP, Paris, France.
[*]These co-authors contributed equally

**Corresponding authors:**
Dr. Stéphanie Gachet, PhD: stephanie.gachet@inserm.fr and Pr. Jean Soulier, MD, PhD: jean.soulier@aphp.fr

[#]Present address : Laboratoire des cellules Souches Hématopoïétiques et des Leucémies, Equipe Niche, Cancer et Radiations dans l'Hématopoïèse, Unité Mixte de Recherche (UMR) 1274-E008, INSERM, CEA, Université Paris-Saclay.

**Running title:**
A relapse-associated program driven by *TP53* alterations in T-ALL

**Keywords:** T-cell acute lymphoblastic leukemia, somatic *TP53* alterations, relapse, leukemia initiating cells, metabolic adaptation, p53 therapeutic targeting, preclinical models

**Footnotes:**

Supplementary informations for this article (Supplementary Figures, 5 and Supplementary Tables, 4) are available online.

**ABSTRACT**

Although most patients with T-cell acute lymphoblastic leukemia (T-ALL) achieve remission with chemotherapy, many relapse with a poor prognosis, treatment-resistant disease. The mechanisms driving chemoresistance remain largely elusive, in part due to the lack of faithful experimental models. Here, we generated isogenic patient-derived xenograft (PDX) pairs at diagnosis and relapse from T-ALL cases harboring *TP53* alterations at relapse (*TP53*$^{alt}$, *TP53* mutation and/or deletion). These models faithfully captured the genomic and functional features of both the diagnosis and the relapse primary leukemias. Despite inter-T-ALL variability, comparative functional analyses revealed a unique, cell-intrinsic relapse phenotype that includes enhanced leukemia-initiating capacity and which can be experimentally conferred to diagnosis cells by *TP53* silencing. Deregulated metabolic pathways and increased MYC signaling are prominent in the relapse phenotype. Ultra-sensitive backtracking of *TP53*-mutant cells and single-cell expression profiling revealed cellular heterogeneity at diagnosis, with sequential progression from a minor subpopulation toward a biallelic *TP53*$^{alt}$ relapse. Our findings support a model in which T-ALL relapse originates from a pre-existing transcriptional state with deregulated metabolism that is selected under therapeutic pressure, opening monitoring prospects for precision medicine.

## INTRODUCTION

T-cell acute lymphoblastic leukemia (T-ALL) is an aggressive hematologic malignancy that represents 15% of pediatric and 25% of all adult ALL cases[1,2]. Multistep deregulation of key transcription factors and additional genes controlling self-renewal, senescence, apoptosis, differentiation or proliferation in a T-cell precursor leads to clonal transformation and expansion of blast cells in the lymphoid organs and the bone marrow[1,3–7]. Although most T-ALL patients at diagnosis achieve remission with intensive chemotherapy and glucocorticoids, 15% to 40% of the patients subsequently experience relapse into a resistant leukemia with dismal prognosis[8–10]. Therefore, comprehensive understanding of the functional mechanisms underlying relapse and resistance is a major unmet need to develop more efficient therapeutic strategies. While exhaustive genetic and immunophenotypic landscape studies have enabled to identify a large variety of T-ALL subtypes[2,7,11,12], these subtypes only partially correlate with the onset of relapse. It rather appears that resistance initiates upon treatment by the selection of residual T-ALL cells with cellular features driving cell survival despite therapy and re-expansion[13–19]. Selection of *NT5C2* somatic mutations leading to cell resistance to 6-mercaptopurine is a well-established, although rare, example of resistance-driven mechanism in T- and B-ALL patients[20–24], and alternative mechanisms remain elusive.

Here, we investigated *TP53* alterations (TP53$^{alt}$, *TP53* mutation and/or deletion) as a factor of resistance acquisition in T-ALL. While rarely detected at diagnosis (2-3%), *TP53*$^{alt}$ is frequently found at relapse (10-25%) and is associated to poor clinical outcomes[25–30]. *TP53*$^{alt}$ cells are genetically trackable, allowing to monitor their functional relapse-associated phenotype. We unveiled a *relapse phenotype* that included increased leukemia initiating activity and modulation of key signaling and metabolic pathways. Sequential selection from a minor cell population expressing this *relapse phenotype* at diagnosis can prime relapse upon therapy.

## RESULTS

### Establishment of isogenic, patient-derived xenografts (PDX) faithfully capturing *TP53*-altered T-ALL diagnosis and relapse genomic patterns

We aimed at uncovering functional mechanisms involved in leukemia resistance and relapse. We focused on *TP53*-altered T-ALL since *TP53* alterations are well-recognized, genetically-trackable, drivers of relapse but are still poorly mechanistically

35 understood in T-ALL[25–29,31]. We selected four cases of T-ALL with *TP53* alterations at
36 relapse only for which cryopreserved diagnosis, remission (i.e., non-tumoral) and
37 relapse patient samples were available. To overcome the limitations of *ex vivo*
38 functional studies on primary samples or cell lines, we established patient-derived
39 xenografts (PDXs) of paired diagnosis (Dx) and relapse (Rel) leukemia in
40 immunodeficient NOD.Cg-*Prkdc*$_{scid}$ *IL2rg*$_{tm1Wjl}$/SzJ (NSG) mice (**Figure 1A**). Genomic
41 analyses of the resulting isogenic, Dx-Rel PDX pairs showed that these PDXs largely
42 captured the genomic pattern of the patient cells, both at diagnosis and at relapse,
43 respectively (**Figure 1B** and **Supplementary Tables 1-2**). *TP53* alterations in patient
44 T-ALL cells were missense mutations in the *TP53* DNA-binding domain within
45 mutational hotspot residues R175 and R248 (cases TALL42; and TALL11 and TALL43,
46 respectively) and a less classical but already reported pathogenic mutation H214 (case
47 TALL30) (**Figure 1C**). The second allele was lost by deletion in 3 cases (TALL30,
48 TALL42 and TALL43) or by 17p unidisomy of the mutated allele in 1 case (TALL11)
49 (**Figure 1B**). The resulting PDXs carried the original *TP53* missense mutations
50 occurring in the DNA-binding domain in association with the loss of the remaining wild-
51 type (WT) allele, as in primary patient samples. Of note, in one T-ALL case, the
52 resulting PDX (PDX43R) captured one of the two *TP53*-altered clones from the relapse
53 patient sample (**Figure 1B**).
54 Interestingly, other somatic CNVs and point mutations (i.e., in addition to *TP53*$^{alt}$) were
55 largely similar in both the diagnosis and relapse samples in the 4 T-ALL pairs,
56 suggesting that *TP53*-driven T-ALL relapse did not display stronger genomic instability
57 (**Figure 1B**).
58 Therefore, these T-ALL PDX models faithfully captured the diagnosis and the relapse
59 patient samples, respectively, enabling further functional comparison experiments
60 using this unlimited ressources of isogenic, human leukemic cells.
61
62 **Relapse cells display a cell-intrinsic, stable, *relapse phenotype* compared to**
63 **their isogenic diagnosis cells**
64 To uncover functional mechanisms involved in leukemia resistance and relapse, we
65 compared the leukemia propagation ability of the diagnosis and relapse T-ALL pairs.
66 First, primary leukemic cells from paired Dx-Rel patient samples were transplanted in
67 parallel at equivalent cell doses in NSG mice, and leukemia onset and mice survival
68 were monitored. Despite strong inter-patient T-ALL heterogeneity, we found in each

69 pair that the relapse cells propagated leukemia more efficiently than their diagnosis
70 counterparts (**Supplementary Figure 1A**), which translated into a significantly shorter
71 mice survival (**Figure 2A** and **Supplementary Figure 1B**). This increased leukemia
72 propagating activity at relapse was conserved in the PDXs established from the 4 pairs.
73 We performed multiple iterative transplantations using decreasing cell doses (**Figures**
74 **2B-C** and **Supplementary Figures 1C-F**) and found that the propagation phenotype
75 was stable upon serial reinjection, without additional acceleration (**Supplementary**
76 **Figures 1D,1F**). Limiting dilution *in vivo* assays (injection of $10^6$ to 1 leukemic
77 cell/mouse) showed that the leukemia initiating cell (LIC) frequencies were increased
78 in the Rel PDXs compared to isogenic Dx counterparts (**Figure 2D** and
79 **Supplementary Table 3**). Consistently, *in vitro* long-term culture-initiating cell assays
80 in coculture with MS5-DL1 stromal cells[32] showed a significantly increased
81 clonogenicity in Rel PDXs from all T-ALL pairs, demonstrating that increased LIC
82 activity is a cell-intrinsic feature of relapse cells (**Supplementary Figure 1G** and
83 **Supplementary Table 3**). Real-time and end-point *in vitro* proliferation using
84 Bromodeoxyuridine (BrdU) pulse labelling and apoptosis experiments, in particular
85 cleaved caspase 3 staining, showed increased proliferation and decreased apoptosis
86 in Rel versus Dx leukemic cells for all tested PDX pairs (**Figures 2E-F** and
87 **Supplementary Figures 1H-I**). Moreover, homing of the leukemic cell in the bone
88 marrow, spleen and liver at 24 hrs was increased in PDXs from Rel for the 4 T-ALL
89 pairs (**Supplementary Figures 1J-K**). However, when homing was bypassed by direct
90 injection of leukemic cells into the femoral bone marrow cavity, leukemic cells from Rel
91 PDXs still propagated leukemia more efficiently than Dx PDXs (**Supplementary**
92 **Figures 1L-M**).
93 Collectively, our data indicate that despite inter-T-ALL heterogeneity, *TP53*$^{alt}$ mediates
94 a unique cell-intrinsic *relapse phenotype* that is associated with increased proliferation,
95 cell survival, and cell homing and post-homing advantage, resulting in higher LIC
96 activity.
97
98 **Experimental *TP53* silencing confers the cell-intrinsic *relapse phenotype* to**
99 **diagnosis leukemia cells**
100 To model *TP53* deregulation as a driver of the *relapse phenotype*, we inactivated *TP53*
101 using a lentiviral shRNA approach in Dx PDX leukemic cells followed by transplantation
102 in NSG mice (**Figure 3A** and **Supplementary Figure 2A**). *TP53* downregulation

103 increased the leukemia propagation capacities of Dx PDX cells when transplanted
104 under parallel and competitive settings (**Figure 3B** and **Supplementary Figures 2B,**
105 **2D-E**), and resulted in enhanced leukemia spreading and shorter survival of the
106 recipient mice (**Figure 3C** and **Supplementary Figure 2C**). This phenotype was
107 retained in secondary transplants, both in parallel and competitive settings (**Figures**
108 **3D-F** and **Supplementary Figures 2F-H**).
109 *In vitro* limiting dilution and proliferation experiments on the *TP53*-silenced Dx PDX
110 cells confirmed the *relapse phenotype*, indicating a *TP53*-dependent increased
111 clonogenic activity (**Figure 3G**, **Supplementary Table 3** and **Supplementary Figure**
112 **2I**).
113 Finally, *in vivo p53*-silenced Dx cells also displayed increased homing and post homing
114 capacities (**Supplementary Figures 2J-M**).
115 Altogether, these results demonstrate that *TP53* silencing confers functional features
116 of the *relapse phenotype* to patient diagnosis cells.
117
118 ***TP53* alterations deregulate MYC signaling and metabolism pathways in T-ALL**
119 **cells and directly contributes to the *relapse phenotype***
120 To dig into the biological pathways deregulated by $TP53^{alt}$ in T-ALL relapse, we
121 compared transcriptional profiles of isogenic Dx and Rel T-ALL PDX samples. While
122 91 genes were upregulated at relapse, 181 genes were downregulated including, as
123 expected, *TP53* itself (except in PDX11R where *TP53* was point-mutated on both
124 alleles) (**Figure 4A** and **Supplementary Figures 3A-B**). Geneset enrichment analysis
125 (GSEA) identified the MYC, E2F, and G2M checkpoint pathways as enriched in Rel
126 cells along with several cell metabolism pathways, including oxidative phosphorylation
127 (OXPHOS), glycolysis and cholesterol homeostasis, defining a *relapse expression*
128 *signature* (**Figure 4B**). Moreover, we interrogated genesets linked to cell proliferation,
129 invasiveness and stemness, and evidenced their upregulation at relapse
130 (**Supplementary Figure 3C**). Analysis in secondary transplant PDXs showed
131 consistent expression patterns, demonstrating functional stability (**Supplementary**
132 **Figures 3D-G** and data not shown). The *relapse expression signature* was also
133 retrieved from the corresponding primary T-ALL samples, further outlining that our Dx-
134 Rel PDX models faithfully captured the features of the patient cells (**Figure 4C**).
135 Considering the role of TP53 in regulating Myc signaling and metabolism
136 pathways[33,34], we focused on OXPHOS and glycolysis and performed real-time

137 measurements of oxygen consumption rate (OCR) and extra cellular acidification rate
138 (ECAR) in isogenic Dx-Rel PDX pairs. We found increased basal and maximal
139 mitochondrial respiration, along with increased glycolysis, in the Rel vs Dx T-ALL cells
140 (**Figures 4D-E** and **Supplementary Figures 3H-K**). Consistently, experimental
141 silencing of *TP53* in the diagnosis PDX cells conferred a relapse mitochondrial and
142 glycolytic profile, demonstrating a driver role of *TP53* inactivation into deregulation of
143 metabolic functions (**Figures 4F-G** and **Supplementary Figures 3L-N**).
144 To evaluate the relevance of the *relapse signature* beyond *TP53* genomic alterations,
145 we analyzed gene expression data from eleven additional primary T-ALL sample pairs
146 lacking *TP53* alterations. Notably, the *relapse expression signature* was enriched in
147 seven of these cases, suggesting that a conserved relapse-associated phenotype may
148 be activated through alternative mechanisms independent of *TP53* genetic alterations.
149 (**Supplementary Figures 3O-P**).
150

151 **Backtracking pre-relapse *TP53*$^{alt}$ clones at diagnosis**

152 As T-ALL relapse can emerge from a minor preexisting subclone at
153 diagnosis[13,17,19,22,35,36], we next aimed to backtrack rare *TP53*-mutated cells that would
154 constitute a pre-relapse reservoir. We performed ultra-high sensitivity approach,
155 namely droplet digital PCR (ddPCR), on the isogenic Dx-Rel primary and PDX
156 samples. We found the expected *TP53* mutation in each case at diagnosis, with mutant
157 allele frequencies corresponding to approximately 1/1300 to 1/5000 total cells, i.e.,
158 below the usual medical diagnosis detection thresholds (**Supplementary Table 4**).
159 This demonstrates the presence in each case of a very minor *TP53*-mutant clone at
160 diagnosis that was further selected in the post-treatment relapse sample. Interestingly,
161 a remission sample was available in one case (TALL11), in which we detected the
162 expected *TP53-p.R248Q* mutation with a frequency of 1 out of 2500 total cells,
163 demonstrating persistence of the cells reservoir after treatment. Strikingly, when the
164 remission sample was injected into NSG mice, a full-blown leukemia developed from
165 these rare cells. All the resulting leukemic cells carried the *TP53-p.R248Q* missense
166 mutation, definitively showing the LIC ability of the minor cell population from
167 diagnosis. However, this leukemia, raised from the remission sample, retained a
168 wildtype allele (*TP53-p.R248Q* allele frequency, 45.7% in sorted leukemia cells) by
169 contrast with the relapse cells that demonstrated copy-neutral loss of the wildtype allele
170 (*TP53-p.R248Q* allele frequency, 91.76%), highlighting the advantage conferred by the

171 monoallelic point mutation in the leukemia expanded from the patient remission sample
172 while the relapse cells displayed an additional loss of the wildtype *TP53* allele with
173 duplication of the *TP53-p.R248Q* allele through acquisition of an uniparental disomy.
174 Those data demonstrates that relapse emerges from a very minor (that is, undetected
175 by standard medical screen) that expands upon therapy with sequential progression
176 towards bi-allelic $TP53^{alt}$ relapse.
177
178 **Single-cell profiling can uncover a pre-relapse minor cell population at diagnosis**
179 **that expresses features of the *relapse phenotype***
180 In an attempt to profile functionally the pre-relapse cell reservoir from diagnosis, we
181 performed single-cell RNAseq analysis on the four T-ALL pairs. The 16 resulting
182 samples (8 primary and 8 from PDXs) did not globally step out by their diagnosis or
183 relapse nature (i.e., all diagnosis *versus* all relapse samples), nor by their origin (i.e.,
184 all primary *versus* all PDX samples), or by cell cycle repartition, but rather by individual
185 T-ALL case (**Figure 5A** and **Supplementary Figures 4A-B**), underlying prominent
186 inter T-ALL biological heterogeneity. GSEA confirmed oxidative phosphorylation
187 signature as the most differentially expressed pathway in all relapse samples along
188 with cell proliferation, cell signaling and cell metabolism pathways (**Supplementary**
189 **Figures 4C-F** and **Figures 5B-C**).
190 Integrated comparison of the diagnosis and relapse samples uncovered a minor cell
191 population in two diagnosis samples that clustered nearby their paired relapse
192 counterparts, suggesting a “pre-relapse” cells reservoir (**Supplementary Figures 4C,**
193 **4E**).
194 *In case TALL42*, the small cluster of cells represented approximately 10% of the total
195 leukemic cells (9.6% and 15% of the primary and the PDX diagnosis samples,
196 respectively) (**Figures 5D-E** and **Supplementary Figures 4G-P**). This cluster was
197 enriched in most of the *relapse expression signature* (**Figure 5F** and **Supplementary**
198 **Figure 4Q**) including OXPHOS, MTORC1 signalling, MYC targets V1, E2F targets,
199 cholesterol homeostasis and DNA repair, these pathways being even more
200 upregulated in the matched relapse cells. In contrast, the G2M checkpoint, MYC target
201 V2 and unfolded protein response (UPR) pathways were downregulated in the minor
202 subclone as compared to the remaining diagnosis cells and to the relapse cells,
203 suggesting an intermediate less proliferative state (**Figure 5F** and **Supplementary**
204 **Figure 4Q**). We interrogated additional geneset collections and found a significant

205 enrichment of stemness, invasiveness and OXPHOS signatures combined with
206 downregulation of cell proliferation pathways in the subclone, in line with the properties
207 attributed to a quiescent LIC-activity enriched, pre-relapse leukemia reservoir (**Figure**
208 **5G** and **Supplementary Figure 4R**). Specifically, interrogation of several leukemia
209 stem cell (LSC) signatures[37–40] showed that the pre-relapse subclone from primary and
210 PDX diagnosis samples had increased LSC signature scores compared to diagnosis
211 cells, as in relapse cells (**Figure 5H**).
212 *In the second case, TALL30*, the deregulation of the *relapse signature* was also
213 detected in a minor subclone at diagnosis. Although this case eventually diverged from
214 the previous T-ALL42 case by the late acquisition of a *NT5C2* mutation, known to drive
215 resistance to maintenance therapy, the initiation of the relapse through a pre-existent
216 population at diagnosis displaying features of the *relapse signature* suggests a
217 common mechanism (**Supplementary Figure 5**).
218 Intriguingly, *TP53* mutation was found in only 0.03% (1 out of 3000) total cells of the
219 two diagnosis samples TALL30 and TALL42, contrasting with approximately 5 and
220 10% of the cells expressing the relapse signature, respectively). Copy-number
221 variations (CNVs) screen using inference analysis showed that the chromosome 17p
222 was not deleted in the pre-relapse subclone in the two cases (**Figure 5I**
223 **Supplementary Figure 4S** and **Supplementary Figure 5H, 5O)**. This suggests that
224 only a small fraction of the minor cell population, i.e. the cells harboring the *TP53*
225 mutation, is further selected towards relapse by chemotherapy, with an additional
226 acquisition of del17p.
227
228
229 **DISCUSSION**
230 Treatment failure and subsequent patient death are largely related to the emergence,
231 within the first 2-years, of a relapse much less responsive to therapies than the initial
232 diagnosis leukemia. Comprehensive longitudinal genomic studies on patient cohorts
233 showed that a few cancer genes can be mutated at T-ALL relapse, *TP53* alterations
234 being the most prominent[25–29]. However, no clear genomic driver of relapse can be
235 detected in most cases and the underlying mechanisms, maybe non-genetic, remain
236 elusive.
237 Here we leveraged *TP53*$^{alt}$ T-ALL relapse cases, i.e. leukemia with a clear, genetically-
238 trackable driver of resistance and relapse to develop faithfull *in vivo* models based on

239 isogenic diagnosis-relapse paired xenografts. Contrasting with many other T-ALL
240 cases where a minor pre-relapse subclone at diagnosis can be selected by the
241 xenotransplantation process[13], our current PDXs faithfully captured the features of both
242 the diagnosis and the relapse T-ALLs, respectively. This substantial difference may be
243 due to the *TP53* lesions nature confering an *in vivo* advantage upon treatment only, as
244 seen in other premalignant conditions[18,41]. Importantly, our isogenic PDX models
245 enable to overcome fundamental limitations of *ex vivo* functional studies on primary
246 samples or cell lines, i.e. rarity and practical workability for primary samples; highly
247 rearranged and drifted cells for cell lines; and, more generally, the absence of a
248 complex microenvironnement crosstalk. In addition, isogenic PDXs also allow to avoid
249 experimental bias related to inter-patient heterogeneity, see for instance the markedly
250 distinct proliferation range between our 4 T-ALL cases, faithfully captured by the PDX
251 isogenic pairs (**Supplementary Figures 1 A-E**).
252 Interestingly, we found that the *TP53*-driven T-ALL relapse cells did not display strong
253 genomic instability features, suggesting a direct oncogenic role of *TP53* alterations in
254 those leukemias as "gatekeeper" rather than its commonly recognized "caretaker" role.
255 This was confirmed by *TP53* silencing experiments evidencing a cell-intrinsic gain of
256 malignancy in relapse cells largely driven by the *TP53* lesion itself. The *relapse*
257 *phenotype* we identied includes a cell-intrinsic functional gain of leukemia initiating
258 activity and proliferation, along with an expression profile that involved cell metabolism,
259 signaling, MYC pathways, and stemness, consistently with a role of *TP53* in the
260 regulation of normal and pathologic stem cell function in hematopoiesis[42]. We
261 especially evidenced that increased p53-dependent OXPHOS was crucial to the
262 *relapse phenotype,* as seen in other acute leukemia subtypes such as acute myeloid
263 leukemia[43]. Collectively, the metabolic *relapse signature* found at relapse, and in pre-
264 relapse minor reservoir at diagnosis, suggests that *TP53* alterations primed T-ALL
265 relapse in a subpopulation resistant to chemotherapy and enriched in LIC activity,
266 along with metabolic and MYC pathway reprogramming.
267 Like in the vast majority of cancers, *TP53*-altered relapses in T-ALL are associated
268 with very poor clinical outcomes and limited therapeutic options, representing a major
269 clinical challenge. While T-ALL stem cell identification by usual immunophenotypic
270 techniques is still debated[44–46,40], our data of a subpopulation resistant to
271 chemotherapy and enriched in LIC activity through enhanced oxidative
272 phosphorylation and MYC pathway activation with concurrent sequential acquisition of

273 bi-allelic *TP53* alterations raises therapeutic propects. Detecting very rare pre-existing
274 *TP53*-mutant cells at diagnosis yields potential strategies of early detection, monitoring
275 and adapted treatment of these cells by early administration of targeted therapies in
276 combination with classical chemotherapy and timely and risk-adapted hematopoietic
277 stem cell transplantation.
278 Interestingly, many T-ALL relapses did not display any additional "relapse-associated
279 genes"[17], suggesting that leukemia resistance and relapse may also be driven by non-
280 genetic mechanisms. In line with this observation, several studies have raised a
281 spectrum of key epigenetic, transcriptionnal remodeling, cell plasticity and
282 microenvironmental/niche mechanisms that may contribute to relapse[17,47,48,35,37,40].
283 Interestingly, the enrichment of the p53-associated *relapse expression signature* in
284 several T-ALL cases lacking *TP53* alterations at relapse suggests that other, possibly
285 epigenetic, mechanisms may activate the *relapse phenotype* we evidenced in this
286 work. This raises the possibility that these biological patterns of resistance may be of
287 wide relevance, including for strategies of early detection, monitoring and targeting of
288 pre-relapse cell populations.
289

290 **METHODS**

291 **Patient cohort, collection of biological material and annotations.** Primary samples
292 from 42 T-ALL patients who have relapsed were obtained from blood or bone marrow
293 (BM) aspirates/biopsies at initial diagnosis, remission (considered as germline
294 reference) and first relapse. The cohort included children and young adults (age, 1 to
295 42 years old). Samples were stored in the Tumor Bank of Saint-Louis Hospital, Paris
296 (BiRTH, Biobank for Research in Translational Hematology) accordingly to the French
297 law, including informed consent. Annotations of T-ALL mutations were obtained using
298 the NGS sequencing and analysis pipeline from Saint-Louis Hospital, using a VAF
299 threshold of 2%[49]. Seven of the 42 patients (16.7%) had *TP53* alterations at relapse,
300 including 4 for which live cells from both diagnosis and relapse could be recovered and
301 injected to mice. IRB approval from the Inserm was given to this study under the
302 number #12–078.

303

304 **Animal studies.** Mice experiments described in this study comply with the current
305 ethical regulations. Authorizations for animal experimentation were obtained from the
306 *Ministère de l'enseignement supérieur et de la recherche* with the No. APAFIS#19958-
307 2019032615074625v2 and APAFIS#47448-2024020909144467v3. Mice were housed
308 under a dark-light cycle at ambient temperature (≈18-23°C) with a humidity of 40-60%
309 and handled in a pathogen-free animal facility in accordance with the guidelines of the
310 Animal Care and Use Committee (IRSL, Université Paris Cité). Animals were excluded
311 from experiments if any sign of stress were observed without clinical signs of full-blown
312 leukemia development (absence of human leukemic cells in blood, bone marrow and
313 spleen).

314

315 **Patient derived xenografts (PDXs) of isogenic diagnosis-relapse T-ALL samples.**
316 Isogenic diagnosis (Dx) and relapse (Rel) T-ALL patient samples were thawed,
317 qualified and injected intravenously (unless otherwise stated) at equivalent cell doses
318 into sublethally irradiated immunodeficient NOD.Cg-Prkdc$_{scid}$ IL2rg$_{tm1Wjl}$/SzJ (NSG)
319 mice from the Jackson Laboratory that are bred locally, as described previously[49].
320 Leukemia development was monitored monthly by flow cytometry (FACS) analysis of
321 blood or BM aspirates using hCD45 and hCD7-based staining protocol detailed in the
322 'Flow cytometry' section to confirm disease engraftment.

323 Human T-ALL cells from both patients and derived PDXs (BM of fully leukemic mice
324 with >95% blasts) were used for genomics, molecular and functional experiments. To
325 evaluate the stability of the phenotype from PDX models, leukemic cells from PDXs at
326 first passage were serially transplanted into NSG recipient mice by intravenous
327 injection (unless otherwise stated) at equivalent cell doses. In some circumstances to
328 evaluate post homing involvement, leukemic cells from isogenic Dx-Rel PDXs were
329 injected into sublethally irradiated mice by intrafemoral route. Recipient mice were
330 monitored daily by visual and clinical observations and monthly for biological
331 parameters, i.e. signs of stress (weakness, weight loss, ruffled coat, lethargy or ataxia)
332 and the presence of human leukemic cells in blood and/or BM. To monitor survival,
333 mice were sacrificed at or before reaching ethical endpoints. Pathology and flow
334 cytometry analyses confirmed full-blown T-ALL disease with marrow, spleen and liver
335 infiltration by leukemic cells.
336
337 **Flow cytometry.** Leukemic cells obtained from peripheral blood after Ficoll separation
338 and from BM aspirates were washed and resuspended in PBS (*Gibco*) supplemented
339 with 2% FBS (*Gibco*) before staining. Human leukemic cells infiltration in NSG recipient
340 mice was measured in legs, spleen and liver that were crushed or mashed. Leukemic
341 cell suspensions were washed and resuspended in PBS supplemented with 2% FBS
342 for staining. Human leukemic cells were then stained for 30 min at 4°C with anti-human
343 CD45 (APC, VioBlue) and CD7 (PE, PE-Vio770) antibodies (*Miltenyi Biotec*) (1:100
344 dilution). Cells were then washed and analysed on a FACS Canto II or LSR Fortessa
345 analyzer (*BD Biosciences*). Flow cytometry analyses were performed using Flowjo
346 10.10 (*TreeStar*).
347
348 **Whole Exome Sequencing Analysis of primary and PDX T-ALL samples.** Primary
349 samples from matched tumoral (initial diagnosis and first relapse) and non-tumoral
350 (remission) obtained from T-ALL patients and the corresponding isogenic Dx-Rel PDXs
351 were subjected to deep whole-exome sequencing (WES). DNA libraries were prepared
352 using SureSelect XT Target Enrichment according to the manufacturer's instructions
353 (*Agilent Technologies*, Santa Clara, CA, USA). Exon capture was performed with
354 Agilent SureSelect Human All Exon V5 kit. The samples were sequenced on an
355 Illumina NextSeq 500 platform (*Illumina*, San Diego, CA, USA) in a 2 × 100 bp paired-
356 end sequencing run. The average sequencing depth was 110X. Raw data were first

357 submitted to quality check using Trim_Galore (v0.6.6) to perform quality and adapter
358 trimming for paired-end reads. The paired end clean reads were aligned to the human
359 reference genome (hg19) using BWA (v0.7.17-r1188). Duplicates reads were flagged
360 using Picard-tools (v2.3.0) and local realignment around InDels and base quality score
361 recalibration was performed using Genome Analysis ToolKit (GATK v4.2.5.0).
362 Somatic mutations were called by VarScan somatic (v2.4.2) and annotated by
363 ANNOVAR (version 2022-04-13) before filtering. Somatic copy number variants
364 (CNVs) were detected by facets (v0.16.0-1) and by an in-house R script. The final
365 retained abnormalities were validated by visual inspection considering a number of
366 markers ≥2 and log2ratio with respect to the individual background noise.
367 Exon capture was performed with Agilent SureSelect Human All Exon V6 UTR kit for
368 the isogenic Dx-Rel PDX pairs. The same procedure as above was used to analyse
369 PDX samples (n= 8) using the corresponding primary non-tumour sample as reference
370 for somatic calling variant step. The overlap between V5 and V6_UTR capture was
371 performed for the upstream analysis.
372
373 ***In vivo* limiting dilution experiments.** Leukemic cells from paired Dx-Rel PDXs
374 (primografts) were intravenously injected under limiting dilution conditions from $10^6$ to
375 1 cell per sublethally irradiated mouse (up to 6 mice per condition). Leukemia
376 development in recipient NSG mice was monitored monthly by blood or BM aspirates.
377 All mice were sacrificed at or before reaching ethical endpoints. Blast infiltration was
378 confirmed as detailed above. Pathology analysis confirmed full-blown T-ALL diagnosis,
379 with BM, spleen and liver infiltration by lymphoblasts expressing human CD45 and
380 CD7 markers. Leukemia initiating cell (LIC) frequencies of isogenic Dx-Rel T-ALL
381 PDXs were calculated from the number of engrafted mice for each cell dose in each
382 condition using the WEHI bioinformatic ELDA (Extreme Limiting Dilution Analysis)
383 software[50]. *P* values were calculated with overall tests for differences in LIC
384 frequencies between any of the group tested.
385
386 ***In vitro* limiting dilution experiment.** Leukemic cells from isogenic Dx-Rel T-ALL
387 PDX samples (primografts) and from paired control mCherry$^+$ and *TP53* KD GFP$^+$ PDX
388 samples at diagnosis were sorted by flow cytometry based on CD45$^+$CD7$^+$ (+/- GFP$^+$
389 or mCherry$^+$) and seeded on irradiated (30 Gy) confluent stromal cells under limiting
390 dilution conditions from 78.125 to 1 cell per well (24 wells per condition). Leukemic

391 cells were then cocultured on stromal feeder cells for 2 to 4 weeks under hypoxic
392 condition (3% $O_2$) as previously described[49]. Cell medium was partially changed twice
393 a week. Positive wells for leukemic cells outgrowth were visually scored at regular time
394 intervals. Leukemic cells detection was confirmed by flow cytometry analysis of
395 recovered wells after 2 to 4 weeks of culture upon hypoxia as detailed above to confirm
396 the presence of leukemic cells. LIC frequencies were calculated from the number of
397 positive wells for leukemic cells outgrowth for each cell dose in each condition using
398 the WEHI bioinformatic ELDA software[50]. *P* values were calculated with overall tests
399 for differences in LIC frequencies between any of the group tested.
400
401 **Real-time measurement of leukemic cells proliferation and apoptosis with the**
402 **IncuCyte® Live-Cell Analysis System.** Real-time measurement of *in vitro* leukemic
403 cell proliferation and apoptosis was performed using the IncuCyte® Live-Cell Analysis
404 System (*Sartorius*). Human $CD45^+CD7^+$ leukemic cells from isogenic Dx-Rel T-ALL
405 PDX samples (primografts) were sorted by flow cytometry and 100.000 cells were
406 seeded on 96-well flat bottom plate (4 wells per condition) previously coated with 0.4μg
407 of purified human Delta4-Fc fusion protein (*PX'Therapeutics*) according to
408 manufacturer's recommendation. Leukemic cells were cultured as previously
409 described[49] for up to 96 hours under normoxia in the IncuCyte® system (5% $CO_2$ and
410 37 °C). Real-time *in vitro* leukemic cell growth was monitored using live-cell time-lapse
411 imaging by capturing phase contrast images every 2 hours and analysed using the
412 integrated confluence algorithm provided. Cell proliferation was represented as the
413 proportion of phase objects confluence over time, without labels. Leukemic cell
414 apoptosis was detected using the IncuCyte® Caspase-3/7 green reagent for apoptosis
415 (*Sartorius*). Briefly, leukemic cells were cultured as previously described in the
416 presence of 5μM Caspase-3/7 green reagent. Real-time live-cell imaging of apoptosis
417 was monitored by capturing phase contrast and green fluorescence images every 2
418 hours and analysed using the integrated algorithm provided. Leukemic cell apoptosis
419 was represented as the proprotion of green fluorescently labelled nuclei after activated
420 caspase-3/7 cleavage of inert Incucyte® Caspase-3/7 dye.
421
422 **Apoptosis and cell proliferation end-point assays.** Leukemic cells from isogenic
423 Dx-Rel PDX T-ALL samples were co-cultured on stromal cells[49] for 48 hours under
424 normoxia in a humidified 5% $CO_2$ incubator at 37°C. To perform apoptosis assay,

425 leukemic cells from co-cultures were then collected, washed and stained as detailed
426 above. Leukemic cells were then fixed and stained with PE or Biotin anti-Cleaved
427 Caspase 3 antibody (*BD Biosciences*) as recommended by the manufacturer's
428 recommendations, washed and then analyzed by flow cytometry on FACS Canto II or
429 a LSR Fortessa analyzers (*BD Biosciences*). Cell cycle assays were performed using
430 the APC BrdU Flow kit (*BD Pharmigen*) as recommended by the manufacturer's
431 recommendations. Briefly, leukemic cells co-cultured on stromal cells for 48 hours
432 were pulse-labeled for one hour at 37°C with 1mM Bromodeoxyuridine (BrdU).
433 Leukemic cells from the recovered co-cultures were stained with cell surface
434 antibodies as above. Leukemic cells were then fixed, permeabilized, incubated with
435 DNase and stained with APC-conjugated anti-BrdU antibody (1:100 dilution) for 20 min
436 at room temperature and incubated with Vybrant violet (1:1000 dilution, *Invitrogen*) for
437 30 min at 37°C before FACS analyses.
438
439 ***In vivo* homing assay.** Leukemic cells from isogenic Dx-Rel PDXs or from matched
440 *TP53*KD and controls Dx PDXs were injected intravenously (2-6x$10^6$ cells/mouse) into
441 sublethally irradiated immunodeficient NSG recipient mice (n = 2 to 4 mice per group).
442 Homing capacities of human leukemic cells were evaluated 24 hours after intravenous
443 injection by FACS analysis of BM, spleen and liver.
444
445 ***TP53* gene silencing in human leukemic cells and *in vivo* transplantations.** The
446 Hu ShRNA anti-*TP53* was previously described[51]. The human *TP53* cDNA was cloned
447 under the H1 promoter in the backbone pRRL.SIN.cPPT.PGK.GFP lentiviral vector
448 (*Addgene* plasmid #22038). The pRRL_H1shCTL_PGK_mCherry lentivector was
449 constructed in house from the pRRL_H1shLacZ_PGK_eGFP mentioned above.
450 Lentiviral particles were produced as described[52] with jetPRIME reagents (*Polyplus*
451 *transfection*) by co-transfection of viral production plasmids, according to the
452 manufacturer's protocol. Lentiviral supernatants titration was performed using the
453 qPCR Lentivirus Titer Kit (*Applied Biological Materials*) according to the manufacturer's
454 recommendation.
455 Leukemic cells from primary PDX samples at diagnosis were cultured on 24-wells
456 plates previously coated with 2.5μg of purified human Delta4-Fc fusion protein
457 (*PX'Therapeutics*) and transduced for 48-72 hours with the lentiviral supernatants
458 including controls (at MOI 20-50) in the presence of 4ug/ml Protamine sulfate (*Sigma*).

459 Transduced leukemic cells were then washed , GFP- and mCherry-FACS sorted and
460 immediately intravenously injected into sub-lethally irradiated NSG mice, at equivalent
461 dose in parallel settings. For competitive experiments, leukemic cells transduced with
462 a shRNA CTL mCherry or shRNA *TP53*-GFP lentivirus were FACS-sorted, and mixed
463 in equivalent number before intravenous injection into sub-lethally irradiated NSG
464 mice. The starting $GFP^+$/$mCherry^+$ ratio was re-checked by flow cytometry before IV-
465 injection. Gene silencing efficiency was checked by immunoblot (human p53 D0-1,
466 *Santa Cruz*; Actin,*Santa Cruz*).
467
468 **Large-scale gene expression analysis of primary and PDX T-ALL samples by**
469 **bulk RNA sequencing analysis.** Total RNAs were extracted from frozen pellets of
470 leukemic blasts at initial diagnosis and first relapse (n= 8 samples) and from BM of fully
471 leukemic NSG mice for the corresponding derived PDXs (n= 24 PDX samples, first
472 injection) using Qiagen RNA extraction kit (*Qiagen,* miRNeasy Tissue cell advance)
473 according to the manufacturer's recommendations. cDNA libraries were prepared
474 using the TruSeq Stranded mRNA kit (*Illumina*, San Diego, CA, USA). Alignment to
475 the hg19 (GRCh37) reference genome was performed using STAR aligner (Version
476 2.7.8a) with quantMode GeneCounts parameter to build raw count matrix for gene-
477 level summarisation based on the in-built hg19 RefSeq-based annotation.
478 Normalisation by the method of trimmed mean of M-values (TMM) was performed
479 using the calcNormFactors function in edgeR. A linear model fitted in limma package
480 was performed to identify differential gene expression between relapse and diagnosis
481 samples in basal conditions. Differentially expressed genes were identified based on
482 the adjusted $p$-value $< 0.05$ and filtered with a fold change absolute value $> 0.5$. The
483 relationship between samples was visualized by hierarchical clustering and principal
484 component analysis (PCA). Over Representation Analysis (ORA) and Gene set
485 enrichment analyses (GSEA) were then performed to identify significant - hallmark,
486 positional (C1), curated (C2), and ontology (C5) - genes sets using the fgsea and
487 msigdbr packages. Additional analyses on PDX samples from secondary transplants
488 were performed using the ClariomTM D Assay plateform (*Thermo Fisher Scientific*)
489 using the manufacturer's recommendations.
490
491 **Mitochondrial Respiration and Glycolytic Function Measurements.** Oxygen
492 consumption rate (OCR) and extracellular acidification rate (ECAR) were respectively

493 measured with the Seahorse XFp Cell Mito Stress and XFp Glycolysis Stress Test kits
494 on the Seahorse XFp Analyser (*Agilent, Seahorse Bioscience*) in accordance with the
495 manufacturer's recommendations. Leukemic cells recovered from 24h co-culture on
496 stromal cells were seeded at 4 x $10^5$ cells per well (optimal cell seeding density was
497 determined in preliminary experiments) in an XFp-well miniplate previously coated with
498 Cell-Tak (*Corning, Fisher Scientific*) in 180µl of XF DMEM Medium (pH 7.4),
499 supplemented with 2 mM L-glutamine (*Gibco*) (for OCR and ECAR), 1 mM fresh
500 sodium pyruvate (*Gibco*) (for OCR only) and 10 mM D-glucose (*Sigma*) (for OCR only)
501 on the day of the assay. For OCR measurements, sequential compound injections of
502 Oligomycin (1µM), FCCP (1µM), Rotenone (0.5 µM) and Antimycin A (0.5µM) enabled
503 measurements of basal respiration, ATP production, proton leak, maximal respiration,
504 spare respiratory capacity, and non-mitochondrial respiration. For ECAR
505 measurements, sequential compound injections of Glucose (10mM), Oligomycin (1µM)
506 and 2-Deoxy-glucose (2-DG, 50mM) enabled measurements of glycolysis, glycolytic
507 capacity, glycolytic reserve and non-glycolytic acidification. Key parameters of
508 mitochondrial respiration and glycolytic functions were recorded for 90 minutes after
509 cells were placed into the analyzer. OCR (pmol/min) and ECAR (mpH/min) were
510 measured simultaneously in all wells, three times at each step, by optical fluorescent
511 O2 sensors, and a minimum of three replicates were analyzed per condition in any
512 given experiment. Unless otherwise stated, all compounds and material were obtained
513 from *Agilent Seahorse Bioscience*.
514
515 **Cell lines and human T-ALL cells culture.** HEK-293T cell line was purchased from
516 ATCC (CRL-3216). HEK-293T cells were grown in DMEM medium (*Gibco*)
517 supplemented with 2mM L-glutamine (*Gibco*), 1% penicillin/streptomycin (*Gibco*), and
518 10% heat-inactivated fetal bovine serum (FBS) (*Gibco*). Mouse MS5-Delta-like1[13,53]
519 and human hTERT-immortalized primary bone marrow MSCs[54] derived stromal cells
520 were maintained in αMEM medium (*Gibco*) supplemented with 2mM L-glutamine
521 (*Gibco*), 1% penicillin/streptomycin (*Gibco*), 1µM Hydrocortisone (*Sigma*, for MSCs
522 only) and 10% heat-inactivated FBS (*Gibco*). All cell lines were grown in a humidified
523 5% $CO_2$ incubator at 37 °C and tested monthly negative for Mycoplasma using
524 MycoAlert PLUS Mycoplasma Detection Kit (*Lonza,*) or MycoStrip Mycoplasma
525 Detection Kit (*Invivogen*).

526 Primary and PDX human T-ALL leukemic cells were cocultured on stromal cells (MS5-
527 DL1 or hMSC cells) in αMEM medium (*Gibco*) supplemented with 2mM L-glutamine
528 (*Gibco*), 1% penicillin/streptomycin (*Gibco*), 10% heat-inactivated FBS (*Stem Cell*
529 *Technologies*), 10% heat-inactivated human AB serum (*Institut de Biotechnologies*
530 *Jacques Boy*), 20nM Human Recombinant Insuline (*SAFC Sigma*), 50ng/ml Human
531 Recombinant SCF (*Miltenyi Biotec*), 10ng/ml Human Recombinant IL7 (*Miltenyi*
532 *Biotec*), 20ng/ml Human Recombinant Flt3 ligand (*Miltenyi Biotec*) as already
533 described[13,49].
534
535 **High-throughput short read single-cell RNA sequencing analysis of paired Dx-**
536 **Rel primary and PDX T-ALL samples.** Single-cell RNA-sequencing (scRNAseq)
537 studies were performed on viable leukemic cells prepared from cryopreserved BM
538 samples from T-ALL patients and the corresponding derived PDXs. Libraries from
539 10.000 leukemic cells were prepared using the Chromium Next GEM Single Cell 3'
540 v3.1 reagent kits (*10x Genomics*) and subjected to short read sequencing on the
541 Illumina NovaSeq 6000 platform (*Illumina*, San Diego, CA, USA) in a 28-8-91 paired-
542 end sequencing run (50.000 reads per cell) allowing the captured expression of ~2000
543 genes per cell. FASTQ files were aligned to the human reference sequence (hg38)
544 using CellRanger count pipeline (*10× Genomics*, v3.1.0). The output gene-barcode
545 matrices were imported into the Seurat R package (v4.3.0) for scRNAseq data analysis
546 and visualization. Cells with nFeature_RNA <500 or >20% mitochondrial genes
547 content were filtered out. After removing of low-quality cells, data were normalized
548 using the Normalized-Data function with "LogNormalize" and a scale factor of 10,000.
549 Highly variable features were identified using the FindVariableFeatures function with
550 selection method "vst". Data were scaled using the ScaleData function and S.Score
551 and G2M.Score obtained from CellCycleScoring function were regressed out. Cells
552 were clustered using FindNeighbors (dims =1:50) with the FindClusters function
553 (resolution =0.6) based on the shared nearest neighbour. Datasets were visualized
554 through non-linear dimensional reduction using the Uniform Manifold Approximation
555 and Projection (UMAP). To identify a list of differentially expressed genes, gene
556 expression comparisons between clusters and/or samples were performed using the
557 fast Wilcoxon rank-sum test and area under the receiver operating characteristic curve
558 (auROC) analysis implemented in the R package Presto (v1.0.0). Gene signature
559 scores were computed using the AddModuleScore_UCell function from the UCell R

560 package (v2.6.2), which applies a rank-based scoring method for robust and scalable
561 analysis. To detect large-scale copy number variations in tumor cells, we utilized the
562 inferCNV package (v1.20.0)[55,56]. Gene expression profiles of all relapse cells, or of a
563 defined subset representing the pre-relapse subclone, were contrasted against
564 diagnostic cells to infer chromosomal variations in tumor cell clusters by analyzing
565 expression intensities across genomic locations and thereby explore potential
566 chromosomal alterations.
567
568 ***TP53*-mutant cells backtracking in isogenic primary and PDX T-ALL samples by**
569 **droplet-digital PCR.**
570 Droplet-digital PCR (ddPCR) reactions were performed following Bio-Rad
571 recommendation's with 2X ddPCR SuperMix for probes No dUTP and commercially
572 designed ddPCR Mutation Assays for each *TP53* mutation (*Bio-Rad*). Mutation assays
573 are a mix of two fluorescent probes in competition for the annealing on the same target
574 sequence: one specific probe for the wild-type sequence (FAM probe) and a HEX
575 probe, specific of the mutated sequence. Two wet-lab validated ddPCR MUT FAMHEX
576 Assay were used for detection of patient's specific mutations (*TP53 p.R175H* (Assay
577 ID dHsaMDV2010105) and *TP53 p.R248Q* (Assay ID dHsaMDV2010127)) and a non-
578 wet-lab validated assay IS ddPCR MUT FAMHEX Assay was used for *TP53 p.H214R*
579 mutation detection (Assay ID dHsaMDS2510824). Experiments were performed on
580 genomic DNA from isogenic primary and PDX T-ALL samples. Several wells were
581 loaded with DNA from each sample to test enough material. Droplets were generated
582 using QX200 Droplet Generator (*Bio-Rad*). PCR reactions were performed on an
583 Eppendorf Nexus Gradient thermocycler following cycling conditions after validation of
584 optimum annealing/extension temperature: 95°C for 10 min, 40 cycles of two steps
585 PCR 94°C for 30 sec, 55°C for 1 min with a 2°C/sec ramping, an enzyme denaturation
586 step at 98°C for 10 min and a final hold at 4°C. FAM and HEX fluorescence's of each
587 droplet were then read on the QX200 Droplet reader. Visualization, analysis and VAFs
588 calculation were performed with QXOne Manager 1.2 Standard edition software (*Bio-*
589 *Rad*). Thresholds for each assay were determined aiming maximum specificity, despite
590 sensitivity and quantification accuracy by only incorporated double-positive droplets of
591 a well when at least a single positive-droplet was spotted to avoid potential false
592 double-negative droplets (none as "rain droplets") in the analysis. Non-template
593 controls containing all reagents and the corresponding amount of carrier DNA to be

594 equivalent to the tested samples were included in the analysis. VAFs were calculated
595 by considering all the wells analysed.
596
597 **Statistical analyses.** Statistical analyses were performed with GraphPad Prism
598 (version 10.3; *GraphPad Software Inc.*) or R packages using Mann-Whitney, Anova,
599 Wilcoxon and Kruskal-Wallis tests, as indicated in figure legends. Unless otherwise
600 stated, the data are expressed as mean±s.d. of $n$=3 or more determinations.
601 For xenotransplantation analysis, Kaplan–Meier survival curves were performed and
602 the statistical significance was determined with the Log-rank (Mantel-Cox) test. Overall
603 survival was defined as the time from cell injection to euthanasia or death at predefined
604 endpoints. Animals were censored if the cause of death/sacrifice was not leukemia
605 related. Number of mice and median survival are indicated into brackets.
606 For limiting dilution assays, statistical analysis was performed using the WEHI
607 bioinformatic ELDA (Extreme Limiting Dilution Analysis) software[50]). Differences were
608 considered statistically significant at $p<0.05$ (*), $p<0.01$ (**), $p<0.001$ (***) or $p<0.0001$
609 (****).
610

611 **Authors' Contributions**

612 Conception and design of the study: SG, EC and JS

613 Development of methodology: SG, SQ, LH and JS

614 Acquisition of data (provided materials and animals, acquired and managed patients,
615 provided facilities): SG, SQ, LH, LM, MP, RK, HB, MB, VP, PF, AB, HD, NB, EC and
616 JS

617 Analysis and interpretation of data (biostatistics, computational analysis, statistical
618 analysis): SG, SQ, LH, LM, MB, FS, EC and JS

619 Writing of the manuscript - original draft preparation, review and editing: SG, HdT and
620 JS

621 Grants acquisition and study supervision: SG and JS

622 All authors critically reviewed the manuscript.

623

624 **Disclosure of potential conflicts of interest**

625 The authors declare no potential conflicts of interest.

626

627 **Acknowledgments**

628 The authors thank Niclas Setterblad, Christelle Doliger, Antonio Alberdi, Sophie
629 Duchez and Claire Maillard from the Technological core facility of the Saint-Louis
630 Research Institut, Inserm UMR1342 / CNRS EMR8000; the ICGex NGS platform of
631 the Curie Institut for high-throughput sequencing of *10X* cDNA librairies.

632

633 **Fundings**

634 This work was supported by grants to Jean Soulier from the ERC St Grant Consolidator
635 #311660, the team FRM 2022 program from the Fondation pour la Recherche
636 Médicale #00107939, the Ligue Contre le Cancer IDF, the Fondation Leucémie Espoir,
637 and by grants to Stéphanie Gachet from the Fondation de France, the Fondation ARC
638 pour la Recherche sur le Cancer (PJA 20191209702), and the Paris Saint-Louis
639 Leukemia Institute program (a grant managed by the French National Research
640 Agency under the France 2030 program, ANR-23-IAHU-0005, Institut de la Leucémie
641 Paris Saint-Louis). The ICGex platform was supported by the grants from the French
642 National Research Agency, the Canceropole Ile-de-France and by tge SiRIC-Curie
643 program.

644

645 **Data-sharing statement**

646 The data that support the findings of this study are available from the corresponding
647 authors, [SG and JS], upon reasonable request.

648

649 **REFERENCES**


650 1. Van Vlierberghe, P. & Ferrando, A. The molecular basis of T cell acute lymphoblastic
651 leukemia. *J Clin Invest* **122**, 3398–406 (2012).
652 2. Buckley, M., Yeung, D. T., White, D. L. & Eadie, L. N. T-cell acute lymphoblastic
653 leukaemia: subtype prevalence, clinical outcome, and emerging targeted treatments.
654 *Leukemia* **39**, 1294–1310 (2025).
655 3. Weng, A. P. *et al.* Activating mutations of NOTCH1 in human T cell acute lymphoblastic
656 leukemia. *Science* **306**, 269–71 (2004).
657 4. Ferrando, A. A. *et al.* Gene expression signatures define novel oncogenic pathways in T
658 cell acute lymphoblastic leukemia. *Cancer Cell* **1**, 75–87 (2002).
659 5. Soulier, J. *et al.* HOXA genes are included in genetic and biologic networks defining
660 human acute T-cell leukemia (T-ALL). *Blood* **106**, 274–86 (2005).
661 6. Girardi, T., Vicente, C., Cools, J. & De Keersmaecker, K. The genetics and molecular
662 biology of T-ALL. *Blood* **129**, 1113–1123 (2017).
663 7. Pölönen, P. *et al.* The genomic basis of childhood T-lineage acute lymphoblastic
664 leukaemia. *Nature* **632**, 1082–1091 (2024).
665 8. Desjonqueres, A. *et al.* Acute lymphoblastic leukemia relapsing after first-line pediatric-
666 inspired therapy: a retrospective GRAALL study. *Blood Cancer J* **6**, e504 (2016).
667 9. Heikamp, E. B. & Pui, C. H. Next-Generation Evaluation and Treatment of Pediatric
668 Acute Lymphoblastic Leukemia. *J Pediatr* **203**, 14-24 e2 (2018).
669 10. Pagliaro, L. *et al.* Acute lymphoblastic leukaemia. *Nat. Rev. Dis. Primer* **10**, 41 (2024).
670 11. Brady, S. W. *et al.* The genomic landscape of pediatric acute lymphoblastic leukemia.
671 *Nat. Genet.* **54**, 1376–1389 (2022).
672 12. Pölönen, P., Mullighan, C. G. & Teachey, D. T. Classification and risk stratification in T-
673 lineage acute lymphoblastic leukemia. *Blood* **145**, 1464–1474 (2025).
674 13. Clappier, E. *et al.* Clonal selection in xenografted human T cell acute lymphoblastic
675 leukemia recapitulates gain of malignancy at relapse. *J Exp Med* **208**, 653–61 (2011).
676 14. Mullighan, C. G. *et al.* Genomic analysis of the clonal origins of relapsed acute
677 lymphoblastic leukemia. *Science* **322**, 1377–80 (2008).
678 15. Tosello, V. *et al.* WT1 mutations in T-ALL. *Blood* **114**, 1038–1045 (2009).
679 16. Anderson, K. *et al.* Genetic variegation of clonal architecture and propagating cells in
680 leukaemia. *Nature* **469**, 356–61 (2011).
681 17. Kunz, J. B. *et al.* Pediatric T-cell lymphoblastic leukemia evolves into relapse by clonal
682 selection, acquisition of mutations and promoter hypomethylation. *Haematologica* **100**,
683 1442–50 (2015).
684 18. Wong, T. N. *et al.* Role of TP53 mutations in the origin and evolution of therapy-related
685 acute myeloid leukaemia. *Nature* **518**, 552–555 (2015).
686 19. Oshima, K. *et al.* Mutational landscape, clonal evolution patterns, and role of RAS
687 mutations in relapsed acute lymphoblastic leukemia. *Proc Natl Acad Sci U A* **113**,
688 11306–11311 (2016).
689 20. Meyer, J. A. *et al.* Relapse-specific mutations in NT5C2 in childhood acute lymphoblastic
690 leukemia. *Nat. Genet.* **45**, 290–294 (2013).
691 21. Tzoneva, G. *et al.* Activating mutations in the NT5C2 nucleotidase gene drive
692 chemotherapy resistance in relapsed ALL. *Nat Med* **19**, 368–71 (2013).
693 22. Tzoneva, G. *et al.* Clonal evolution mechanisms in NT5C2 mutant-relapsed acute
694 lymphoblastic leukaemia. *Nature* **553**, 511–514 (2018).
695 23. Dieck, C. L. *et al.* Structure and Mechanisms of NT5C2 Mutations Driving Thiopurine
696 Resistance in Relapsed Lymphoblastic Leukemia. *Cancer Cell* **34**, 136-147.e6 (2018).
697 24. Barz, M. J. *et al.* Subclonal NT5C2 mutations are associated with poor outcomes after
698 relapse of pediatric acute lymphoblastic leukemia. *Blood* **135**, 921–933 (2020).
699 25. Diccianni, M. B. *et al.* Clinical significance of p53 mutations in relapsed T-cell acute
700 lymphoblastic leukemia. *Blood* **84**, 3105–12 (1994).

26. Hof, J. *et al.* Mutations and deletions of the TP53 gene predict nonresponse to treatment and poor outcome in first relapse of childhood acute lymphoblastic leukemia. *J Clin Oncol* **29**, 3185–93 (2011).
27. Hof, J. *et al.* NOTCH1 mutation, TP53 alteration and myeloid antigen expression predict outcome heterogeneity in children with first relapse of T-cell acute lymphoblastic leukemia. *Haematologica* **102**, e249–e252 (2017).
28. Richter-Pechańska, P. *et al.* Identification of a genetically defined ultra-high-risk group in relapsed pediatric T-lymphoblastic leukemia. *Blood Cancer J.* **7**, e523 (2017).
29. Simonin, M. *et al.* Prognostic value and oncogenic landscape of TP53 alterations in adult and pediatric T-ALL. *Blood* **141**, 1353–1358 (2023).
30. Kempter, T. *et al.* Subclonal TP53 and KRAS variants combined with poor treatment response identify ultrahigh-risk pediatric patients with T-ALL. *Blood Adv.* **9**, 1267–1279 (2025).
31. Li, B. *et al.* Therapy-induced mutations drive the genomic landscape of relapsed acute lymphoblastic leukemia. *Blood* https://doi.org/10.1182/blood.2019002220 (2020) doi:10.1182/blood.2019002220.
32. Armstrong, F. *et al.* NOTCH is a key regulator of human T-cell acute leukemia initiating cell activity. *Blood* **113**, 1730–1740 (2009).
33. Liu, Y., Su, Z., Tavana, O. & Gu, W. Understanding the complexity of p53 in a new era of tumor suppression. *Cancer Cell* **42**, 946–967 (2024).
34. Dong, Y., Tu, R., Liu, H. & Qing, G. Regulation of cancer cell metabolism: oncogenic MYC in the driver's seat. *Signal Transduct. Target. Ther.* **5**, 124 (2020).
35. Richter-Pechańska, P. *et al.* Pediatric T-ALL type-1 and type-2 relapses develop along distinct pathways of clonal evolution. *Leukemia* **36**, 1759–1768 (2022).
36. Albertí-Servera, L. *et al.* Single-cell DNA amplicon sequencing reveals clonal heterogeneity and evolution in T-cell acute lymphoblastic leukemia. *Blood* **137**, 801–811 (2021).
37. Calvo, J. *et al.* High CD44 expression and enhanced E-selectin binding identified as biomarkers of chemoresistant leukemic cells in human T-ALL. *Leukemia* **39**, 323–336 (2025).
38. Xu, J. *et al.* A multiomic atlas identifies a treatment-resistant, bone marrow progenitor-like cell population in T cell acute lymphoblastic leukemia. *Nat. Cancer* **6**, 102–122 (2025).
39. Ebinger, S. *et al.* Characterization of Rare, Dormant, and Therapy-Resistant Cells in Acute Lymphoblastic Leukemia. *Cancer Cell* **30**, 849–862 (2016).
40. Costea, J. *et al.* Role of stem-like cells in chemotherapy resistance and relapse in pediatric T-cell acute lymphoblastic leukemia. *Nat. Commun.* **16**, 5413 (2025).
41. Hsu, J. I. *et al.* PPM1D Mutations Drive Clonal Hematopoiesis in Response to Cytotoxic Chemotherapy. *Cell Stem Cell* **23**, 700-713.e6 (2018).
42. Chen, S. *et al.* Mutant p53 drives clonal hematopoiesis through modulating epigenetic pathway. *Nat. Commun.* **10**, 5649 (2019).
43. Rodriguez-Zabala, M. *et al.* Combined GLUT1 and OXPHOS inhibition eliminates acute myeloid leukemia cells by restraining their metabolic plasticity. *Blood Adv.* **7**, 5382–5395 (2023).
44. Chiu, P. P. L., Jiang, H. & Dick, J. E. Leukemia-initiating cells in human T-lymphoblastic leukemia exhibit glucocorticoid resistance. *Blood* **116**, 5268–5279 (2010).
45. Belmonte, M., Hoofd, C., Weng, A. P. & Giambra, V. Targeting leukemia stem cells: which pathways drive self-renewal activity in T-cell acute lymphoblastic leukemia? *Curr Oncol* **23**, 34–41 (2016).
46. Gerby, B. *et al.* High-throughput screening in niche-based assay identifies compounds to target preleukemic stem cells. *J. Clin. Invest.* **126**, 4569–4584 (2016).
47. Yadav, B. D. *et al.* Heterogeneity in mechanisms of emergent resistance in pediatric T-cell acute lymphoblastic leukemia. *Oncotarget* **7**, 58728–42 (2016).
48. Ariës, I. M. *et al.* PRC2 loss induces chemoresistance by repressing apoptosis in T cell acute lymphoblastic leukemia. *J. Exp. Med.* **215**, 3094–3114 (2018).

49. Gachet, S. *et al.* Deletion 6q Drives T-cell Leukemia Progression by Ribosome Modulation. *Cancer Discov* **8**, 1614–1631 (2018).
50. Hu, Y. & Smyth, G. K. ELDA: extreme limiting dilution analysis for comparing depleted and enriched populations in stem cell and other assays. *J. Immunol. Methods* **347**, 70–78 (2009).
51. Ceccaldi, R. *et al.* Bone marrow failure in Fanconi anemia is triggered by an exacerbated p53/p21 DNA damage response that impairs hematopoietic stem and progenitor cells. *Cell Stem Cell* **11**, 36–49 (2012).
52. Sebert, M. *et al.* Clonal hematopoiesis driven by chromosome 1q/MDM4 trisomy defines a canonical route toward leukemia in Fanconi anemia. *Cell Stem Cell* **30**, 153-170.e9 (2023).
53. Gerby, B. *et al.* Optimized gene transfer into human primary leukemic T cell with NOD-SCID/leukemia-initiating cell activity. *Leukemia* **24**, 646–9 (2010).
54. Mihara, K. *et al.* Development and functional characterization of human bone marrow mesenchymal cells immortalized by enforced expression of telomerase. *Br. J. Haematol.* **120**, 846–849 (2003).
55. Patel, A. P. *et al.* Single-cell RNA-seq highlights intratumoral heterogeneity in primary glioblastoma. *Science* **344**, 1396–1401 (2014).
56. Zhu, Q. *et al.* Single cell multi-omics reveal intra-cell-line heterogeneity across human cancer cell lines. *Nat. Commun.* **14**, 8170 (2023).

## FIGURE LEGENDS

**Figure 1. *In vivo* isogenic modelling of diagnosis and relapse *TP53*-altered T-ALL. A.** Experimental design (Created in BioRender. Gachet, S. (2026) https://BioRender.com/zczr8er). Isogenic Dx-Rel PDX pairs were established after injection into immunodeficient NSG mice of paired primary diagnosis and *TP53*-altered (*TP53*$^{alt}$) relapse samples from the same T-ALL patients. **B.** Comparative Whole Exome Sequencing (WES) analysis of the isogenic Dx-Rel PDX samples established from 4 T-ALL patients who relapsed with *17p/TP53* alterations. In each case, PDX samples (PDXD and PDXR) are compared side-by-side to the corresponding primary samples (TALLD and TALLR, respectively). **C.** Lollipop plot of TP53 mutations observed in four primary relapse samples (TALL11R, TALL30R, TALL42R and TALL43R).

**Figure 2. *TP53*$^{alt}$ T-ALL relapse cells display a cell-intrinsic gain of malignancy phenotype. A.** Kaplan-Meier survival curves of PDX mice engrafted with primary isogenic Dx-Rel leukemic cells from 4 T-ALL patients (TALL11, TALL30, TALL42 and TALL43). N=4-5 recipient mice injected at equivalent cell doses per sample. **B-C.** Parallel serial transplantations of paired Dx-Rel T-ALL PDX samples. Kaplan-Meier survival curves of mice injected with 3 cell doses ($10^6$, $10^5$ and $10^4$ cells) of isogenic Dx-Rel PDX pairs (n = 4 TALL cases) raised from primary (**B**) and secondary (**C**) xenografts. **D.** LIC frequencies of isogenic Dx-Rel PDX sample pairs calculated from *in vivo* limiting dilutions. **E-F.** Real-time *in vitro* cell proliferation and apoptosis of leukemic cells from isogenic Dx-Rel PDX pairs, measured with the Incucyte® Live-Cell Analysis System. Proliferation was quantified by measuring the proportion of phase objects confluence over time, without labels **(E)**, and apoptosis by the quantification of green fluorescently labelled nuclei after activated caspase-3/7 cleavage of inert Incucyte® Caspase-3/7 dyes **(F)**.

Statistical data in this figure are represented as mean ± s.d. Significance is indicated by *P* values; A-C: Log-rank test (Mantel-Cox); D: overall tests for differences using ELDA software; E-F: two-way Anova test. Number of recipient mice and median survival are indicated into brackets on Kaplan-Meier survival curves. ns, not significant; *, $p < 0.05$; **, $p < 0.01$; ***, $p < 0.001$; ****, $p < 0.0001$.

811 **Figure 3. *TP53* silencing confers a *relapse phenotype* to diagnosis leukemic**
812 **cells. A.** Experimental design of *TP53* silencing in diagnosis cells from PDX samples
813 using a lentiviral shRNA approach (Created in BioRender. Gachet, S. (2026)
814 https://BioRender.com/usb6t9c). **B-C.** Primary transplantation of paired control
815 mCherry$^+$ (shCTL mCherry) and *TP53* KD GFP$^+$ (sh *TP53* GFP) leukemic cells from
816 PDX30D injected in parallel settings into recipient mice. **B.** Engraftment kinetics in the
817 bone marrow (BM) of recipient mice (n=6) injected with paired control and *TP53* KD
818 leukemic cells from PDX30D. **C.** Kaplan-Meier survival curves of mice injected with
819 paired control and *TP53* KD leukemic cells from PDX30D. **D-F.** Secondary transplant
820 of paired control mCherry$^+$ (shCTL mCherry) and *TP53* KD GFP$^+$ (sh *TP53* GFP)
821 leukemic cells from PDX30D injected either in parallel (panels D-E) or competitive
822 (panel F) settings into recipient mice. **D.** Engraftment kinetics in the BM of recipient
823 mice (n=5) injected in parallel settings with cells from control and *TP53* KD conditions.
824 **E.** Kaplan-Meier survival curves of mice injected in parallel settings with sorted control
825 or *TP53* KD leukemic cells from PDX30D. **F.** Engraftment kinetics in the BM of recipient
826 mice (n=4) injected with sorted cells from both control and *TP53* KD in competitive
827 settings (ratio 1:1). Data are represented as ratios of *TP53* KD GFP$^+$ over control
828 mCherry$^+$ leukemic cells within BM of the same recipient mouse and compared to the
829 input. **G.** LIC frequencies of paired control-*TP53* KD samples calculated from *in vitro*
830 limiting dilutions of sorted GFP$^+$ or mCherry$^+$ CD45$^+$CD7$^+$ leukemic cell from diagnosis
831 PDX samples (PDX30D and PDX42D). LIC frequencies are estimated based on the
832 proportions of positive wells for GFP$^+$/mCherry$^+$ CD45$^+$CD7$^+$ leukemic cells evaluated
833 after 2 and 4 weeks of culture.
834 Statistical data in this figure are represented as mean ± s.d. Significance is indicated
835 by *P* values; B and D: Mann-Whitney test; C and E: Log-rank test (Mantel-Cox); F:
836 Kruskal-Wallis test; G: overall tests for differences using ELDA software. Number of
837 recipient mice and median survival are indicated into brackets on Kaplan-Meier
838 survival curves. ns, not significant; *, $p < 0.05$; **, $p < 0.01$; ****, $p < 0.0001$.
839
840 **Figure 4. *TP53* alterations drive a *relapse phenotype* through MYC signaling and**
841 **metabolism deregulation. A.** Supervised hierarchical clustering of the top fifty most
842 differentially expressed genes between Dx and Rel T-ALL samples. Heatmap
843 representation of the most variables genes at Dx and Rel in 4 isogenic PDX pairs
844 (primografts). *TP53* expression is highlighted in red. Independent triplicates are

845 analysed for each isogenic PDX pair. **B-C.** GSEA of enriched pathways in *TP53*$^{alt}$ T-
846 ALL relapse samples. **B.** Comparative Gene Set Enrichment Analysis (GSEA) of
847 differentially expressed genes in Rel and Dx samples from 4 isogenic PDX pairs.
848 Representation of selected Hallmark pathways significantly upregulated at relapse,
849 defining a *relapse expression signature* in all isogenic Dx-Rel PDX pairs pooled
850 together (1$^{st}$ column "All_PDXs") and in each individual PDX pair (2$^{nd}$ to 5$^{th}$ columns;
851 respectively PDX11, PDX30, PDX42 and PDX43) (*P* adj <0.05). **C.** GSEA of the
852 upregulated (upper panel) and downregulated (lower panel) *relapse expression*
853 *signature* obtained from PDX samples (panel B) tested in the original T-ALL patients
854 samples. UP_PDX, upregulated transcriptomic signature in Rel PDXs; DOWN_PDX,
855 downregulated transcriptomic signature in Rel PDXs. FDR, false discovery rate; NES,
856 normalized enrichment score. **D-G.** Direct evaluation of mitochondrial respiration in
857 leukemic cells from isogenic Dx-Rel PDXs using Seahorse assays. **D.** Real-time
858 measurements of oxygen consumption rate (OCR) in isogenic Dx-Rel leukemic cells
859 from 4 T-ALL cases. **E.** Quantification of maximal respiration in leukemic cells from 4
860 isogenic Dx-Rel PDX pairs evaluated in 3 independent experiments. **F.** Real-time
861 measurements of OCR in *TP53*-silenced (*TP53* KD) and matched control leukemic
862 cells from diagnosis PDX samples (PDX42D and PDX43D). **G.** Quantification of
863 maximal respiration in *TP53* KD and control leukemic cells from 3 independent
864 diagnosis PDX samples (PDX30D, PDX42D and PDX43D) evaluated in 2 independent
865 experiments
866 Statistical data in this figure are represented as mean ± s.d. Significance is indicated
867 by *P* values; E and G: Mann-Whitney test. ns, not significant; **, $p < 0.01$; ***, $p <$
868 $0.001$; ****, $p < 0.0001$.
869
870 **Figure 5. Single-cell profiling of isogenix Dx-Rel T-ALLs can unveil a minor pre-**
871 **relapse subclone at diagnosis. A.** UMAP visualizations of isogenic Dx-Rel primary
872 samples from 4 T-ALL patients and their derived PDXs analysed by short read single-
873 cell RNA (scRNA) sequencing. UMAP plots of 117.119 single cells coloured by T-ALL
874 samples (n=16, primary and PDXs samples from four T-ALL cases at diagnosis and
875 relapse; left panel), leukemic cell identity (Diagnosis versus Relapse; middle panel)
876 and by leukemic cell origin (Primary versus PDX; right panel). **B-C.** GSEA of biological
877 pathways enriched at relapse in primary and PDX T-ALL samples. GSEA from pseudo
878 bulk analysis of differentially expressed genes between relapse (Rel) and diagnosis

879 (Dx) samples from isogenic patient (**B**) and PDX (**C**) T-ALL pairs retrieves the *relapse*
880 *expression signature* defined in Figure 4B. Representation of selected Hallmark
881 pathways significantly deregulated at relapse (*P* adj <0.05) in all isogenic pairs pooled
882 together (1st column ") and in each individual pair (2nd to 5th columns). **D.** UMAP
883 visualizations of Dx and Rel primary samples from TALL42 case analysed by short
884 read scRNA sequencing. UMAP plots of 14.049 single leukemic cells coloured by cell
885 identity (Diagnosis vs Relapse; upper panel) and cluster-based by transcriptomic data
886 (fourteen different clusters; lower panel). The red dotted ellipse highlights cluster 6 in
887 TALL42D sample. **E.** Dot plot visualization of biomarker genes average expression
888 selected from the unsupervised differential expression analysis between Rel and Dx
889 samples from TALL42 case. Average expression and proportion of expressing cells for
890 selected biomarkers are represented in each cluster from Dx and Rel samples. The
891 red dotted line highlights the "pre-relapse" clone. **F-G.** GSEA of positively and
892 negatively enriched pathways at relapse and "pre-relapse" stages in TALL42 samples.
893 **F.** Representation of selected Hallmark pathways significantly deregulated in relapse
894 (1st column Rel vs Dx; *P* adj <0.05) and "pre-relapse" (2nd column Sub vs Dx, red dotted
895 line; *P* adj <0.05) clusters as compared to matched diagnosis counterparts. **G.**
896 Representation of specific gene sets from the MSigDB C1 and C2 collections
897 significantly upregulated (in red) or downregulated (in blue) at relapse (1st column Rel
898 vs Dx; *P* adj <0.05) and "pre-relapse" (2nd column Sub vs Dx; *P* adj <0.05) as compared
899 to matched primary diagnosis counterparts. Color code indicates the cell proliferation,
900 invasiveness, stemness and oxidative phosphorylation signatures. **H.** Single-cell
901 scores for several leukemia stem cell (LSC) signatures in TALL42 diagnosis (Dx), pre-
902 relapse (Sub) and relapse (Rel) clusters. The box includes the median, hinges mark
903 the 25th and 75th percentiles. *P* values from a two-sided paired t-test are shown. ns,
904 not significant; ****, $p < 0.0001$ **I.** CNV inference analysis of cluster 6 ('Sub'; "pre-
905 relapse" subpopulation) from TALL42D and all the clusters from TALL42R (clusters 0,
906 3, 4 and 9; 'Rel') interrogating copy number alterations on each chromosome (lower
907 part) as compared to the remaining diagnosis sample (clusters 1, 2, 5, 7, 10 and 11;
908 'Dx') as a reference (upper part). The red circle highlights the CNV status for
909 chromosome 17p in the pre-relapse clone (cluster 6) from TALL42D.
910

# Figure 1

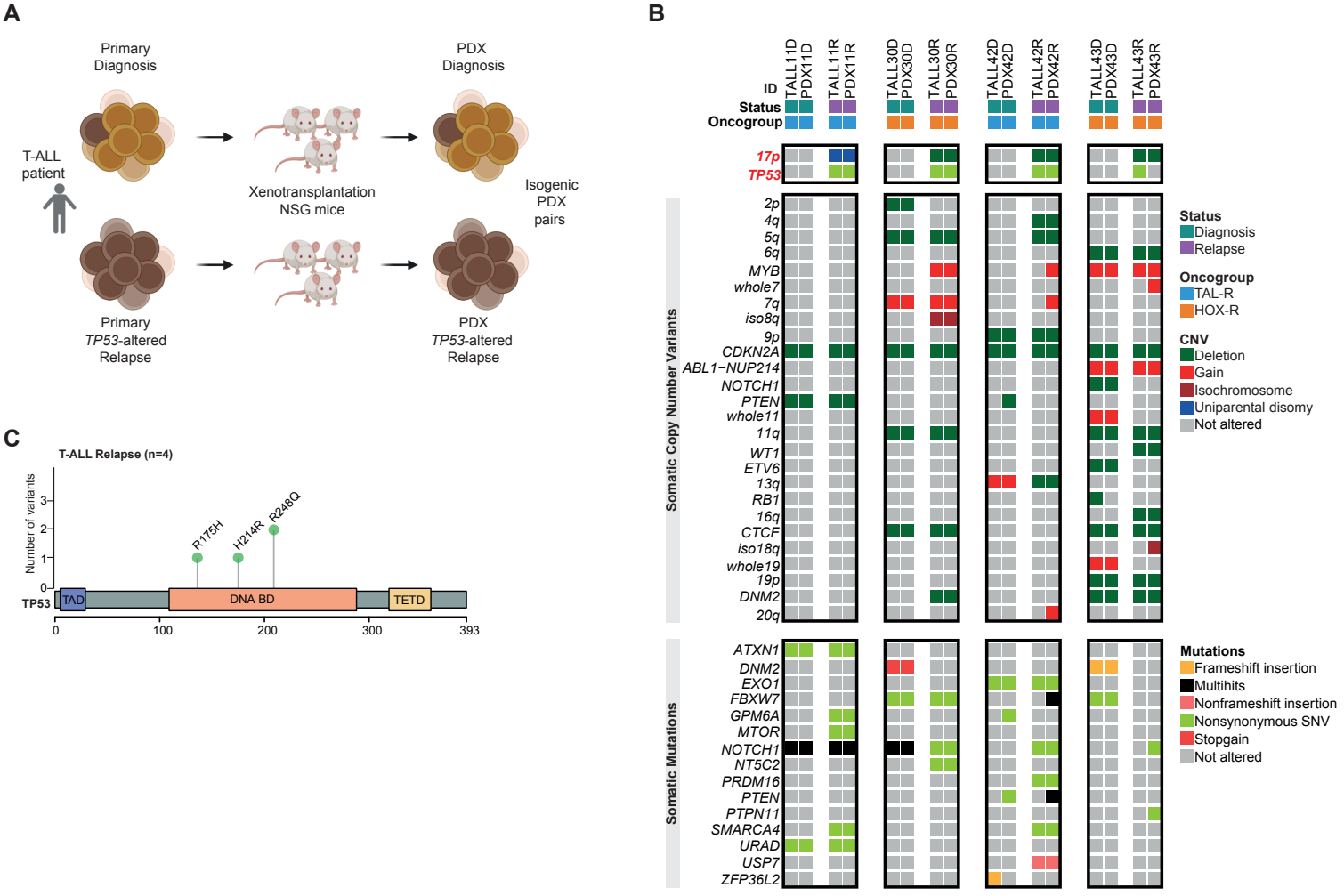
A
Primary Diagnosis
PDX Diagnosis
T-ALL patient
Xenotransplantation NSG mice
Isogenic PDX pairs
Primary TP53-altered Relapse
PDX TP53-altered Relapse
B
ID
Status
Oncogroup
TALL11D PDX11D
TALL11R PDX11R
TALL30D PDX30D
TALL30R PDX30R
TALL42D PDX42D
TALL42R PDX42R
TALL43D PDX43D
TALL43R PDX43R
17p
TP53
Somatic Copy Number Variants
2p
4q
5q
6q
MYB
whole7
7q
iso8q
9p
CDKN2A
ABL1−NUP214
NOTCH1
PTEN
whole11
11q
WT1
ETV6
13q
RB1
16q
CTCF
iso18q
whole19
19p
DNM2
20q
Somatic Mutations
ATXN1
DNM2
EXO1
FBXW7
GPM6A
MTOR
NOTCH1
NT5C2
PRDM16
PTEN
PTPN11
SMARCA4
URAD
USP7
ZFP36L2
Status
Diagnosis
Relapse
Oncogroup
TAL-R
HOX-R
CNV
Deletion
Gain
Isochromosome
Uniparental disomy
Not altered
Mutations
Frameshift insertion
Multihits
Nonframeshift insertion
Nonsynonymous SNV
Stopgain
Not altered
C
T-ALL Relapse (n=4)
Number of variants
R175H
H214R
R248Q
TP53
TAD
DNA BD
TETD
0
100
200
300
393

# Figure 2

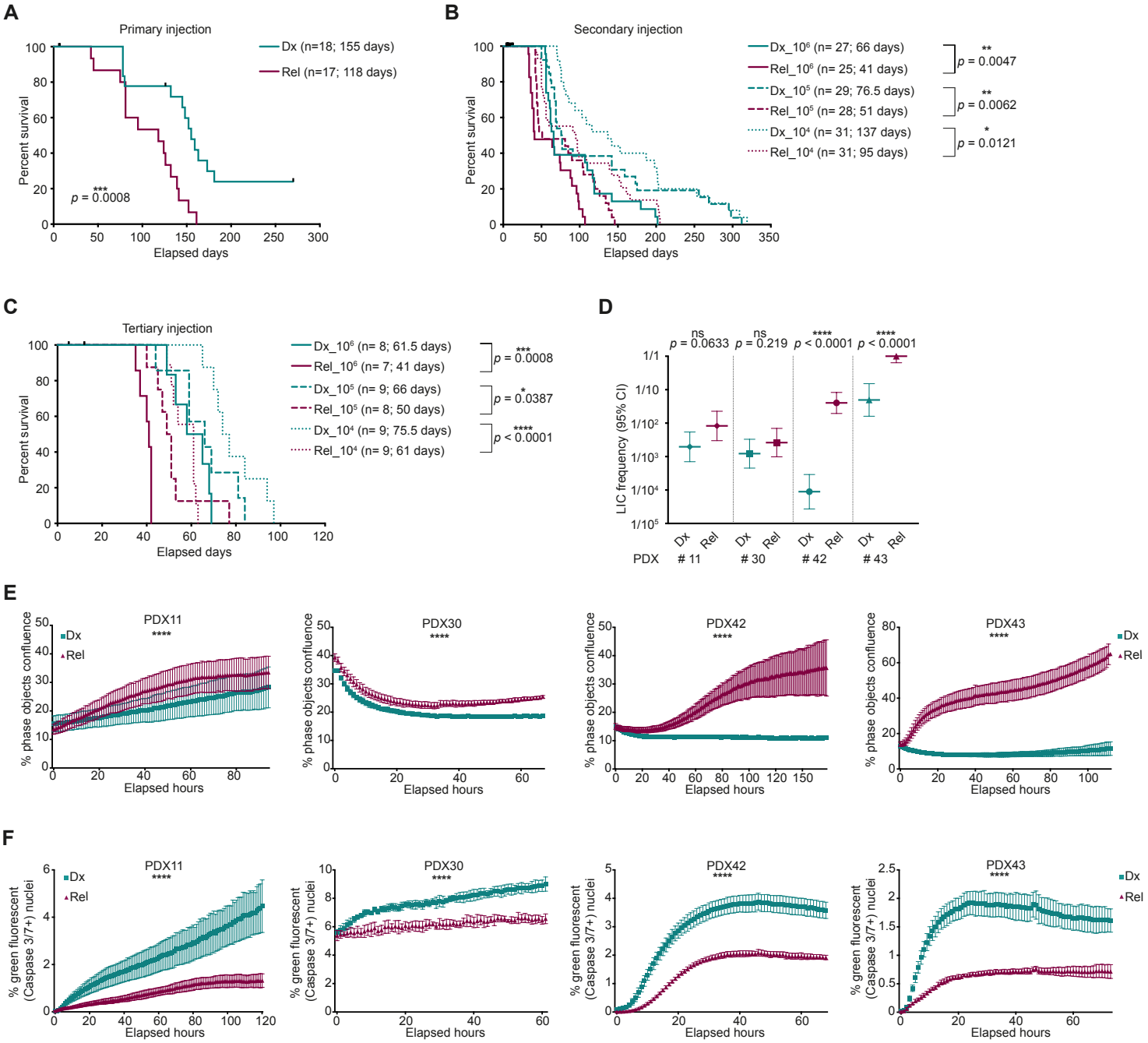
A
Primary injection
Dx (n=18; 155 days)
Rel (n=17; 118 days)
Percent survival
Elapsed days
p = 0.0008
B
Secondary injection
Dx_10⁶ (n= 27; 66 days)
Rel_10⁶ (n= 25; 41 days)
Dx_10⁵ (n= 29; 76.5 days)
Rel_10⁵ (n= 28; 51 days)
Dx_10⁴ (n= 31; 137 days)
Rel_10⁴ (n= 31; 95 days)
p = 0.0047
p = 0.0062
p = 0.0121
C
Tertiary injection
Dx_10⁶ (n= 8; 61.5 days)
Rel_10⁶ (n= 7; 41 days)
Dx_10⁵ (n= 9; 66 days)
Rel_10⁵ (n= 8; 50 days)
Dx_10⁴ (n= 9; 75.5 days)
Rel_10⁴ (n= 9; 61 days)
p = 0.0008
p = 0.0387
p < 0.0001
D
p = 0.0633
p = 0.219
p < 0.0001
p < 0.0001
LIC frequency (95% CI)
PDX # 11 # 30 # 42 # 43
E
PDX11
PDX30
PDX42
PDX43
% phase objects confluence
Elapsed hours
Dx
Rel
F
% green fluorescent (Caspase 3/7+) nuclei
Elapsed hours

# Figure 3

**A**

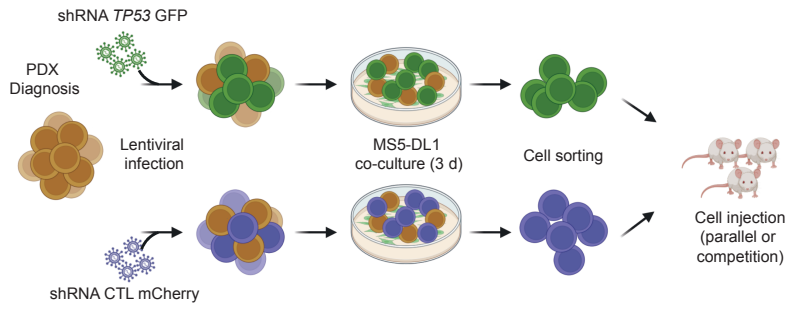


**B**

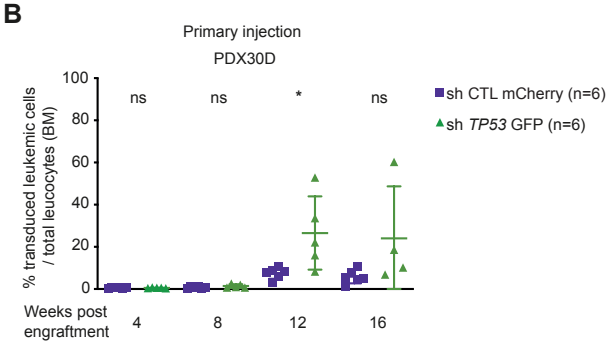


**C**

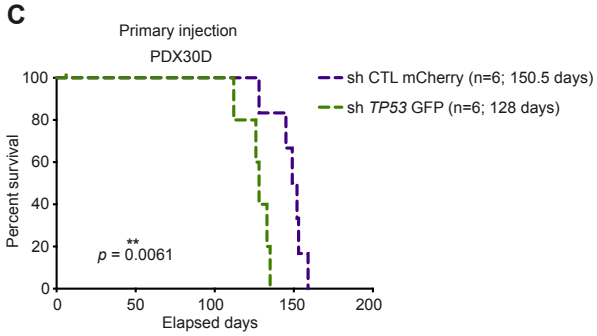


**D**

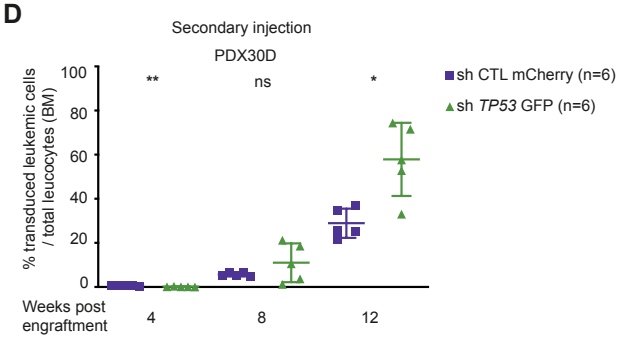


**E**

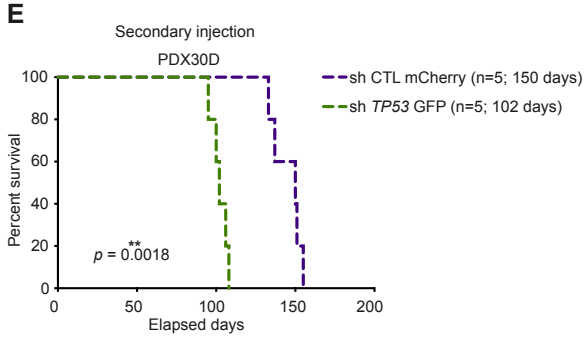


**F**

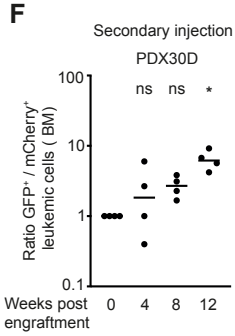


**G**

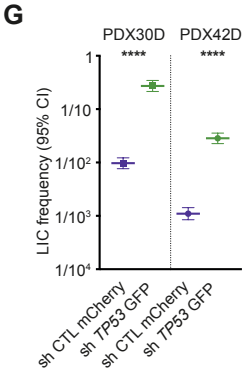

# Figure 4

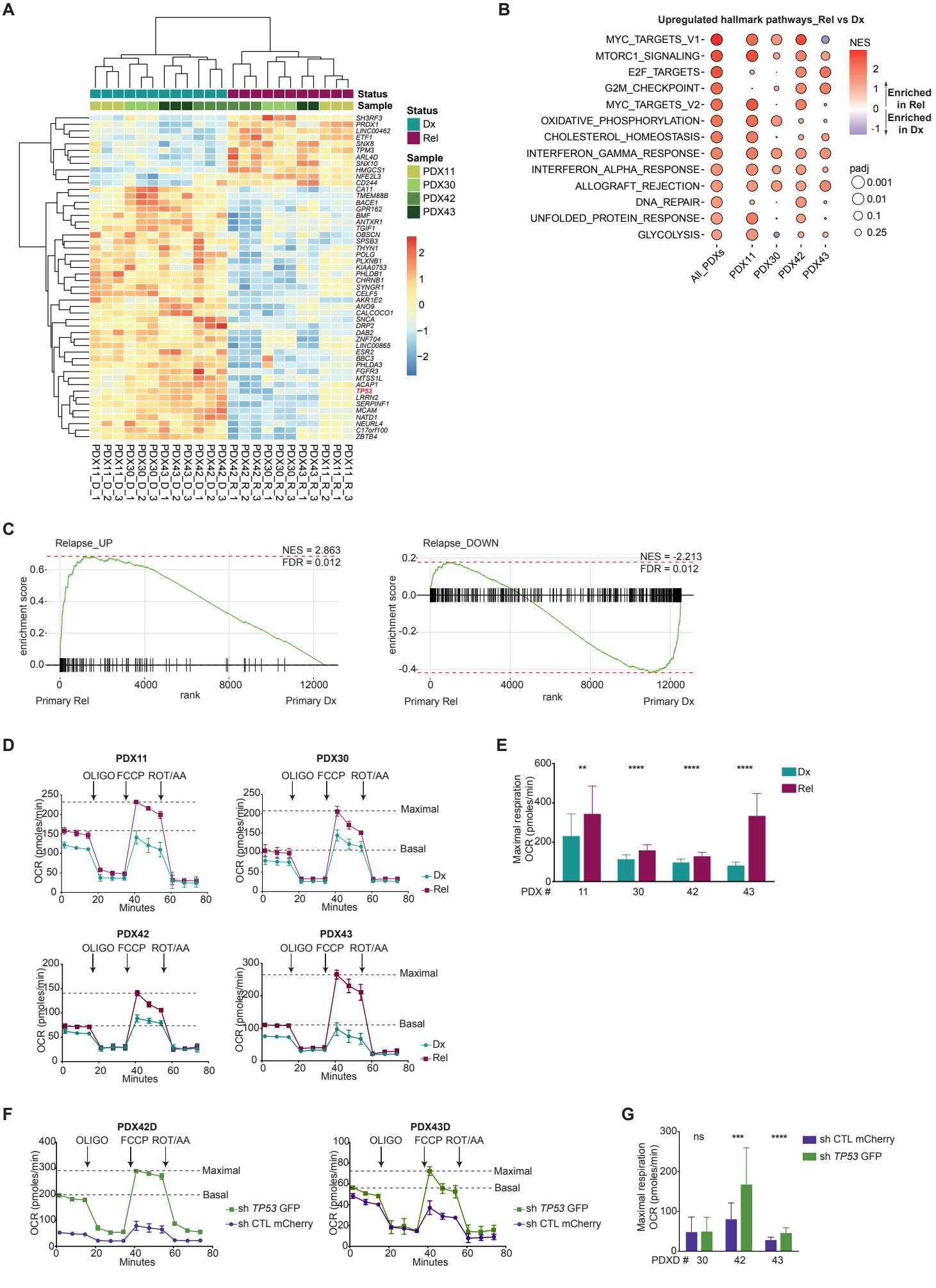
A
Status
Sample
Status
Dx
Rel
Sample
PDX11
PDX30
PDX42
PDX43
SH3RF3
PRDX1
LINC00462
ETF1
SNX8
TPM3
ARL4D
SNX10
HMGCS1
NFE2L3
CD244
CA11
TMEM88B
BACE1
GPR162
BMF
ANTXR1
TGIF1
OBSCN
SPSB3
THYN1
POLG
PLXNB1
KIAA0753
PHLDB1
CHRNB1
SYNGR1
CELF5
AKR1E2
ANO9
CALCOCO1
SNCA
DRP2
DAB2
ZNF704
LINC00865
ESR2
BBC3
PHLDA3
FGFR3
MTSS1L
ACAP1
TP53
LRRN2
SERPINF1
MCAM
NATD1
NEURL4
C17orf100
ZBTB4
PDX11_D_1
PDX11_D_2
PDX11_D_3
PDX30_D_1
PDX30_D_2
PDX30_D_3
PDX43_D_1
PDX43_D_2
PDX43_D_3
PDX42_D_1
PDX42_D_2
PDX42_D_3
PDX42_R_1
PDX42_R_2
PDX42_R_3
PDX30_R_1
PDX30_R_2
PDX30_R_3
PDX43_R_1
PDX43_R_2
PDX43_R_3
PDX11_R_1
PDX11_R_2
PDX11_R_3
B
Upregulated hallmark pathways_Rel vs Dx
MYC_TARGETS_V1
MTORC1_SIGNALING
E2F_TARGETS
G2M_CHECKPOINT
MYC_TARGETS_V2
OXIDATIVE_PHOSPHORYLATION
CHOLESTEROL_HOMEOSTASIS
INTERFERON_GAMMA_RESPONSE
INTERFERON_ALPHA_RESPONSE
ALLOGRAFT_REJECTION
DNA_REPAIR
UNFOLDED_PROTEIN_RESPONSE
GLYCOLYSIS
All_PDXs
PDX11
PDX30
PDX42
PDX43
NES
Enriched in Rel
Enriched in Dx
padj
0.001
0.01
0.1
0.25
C
Relapse_UP
NES = 2.863
FDR = 0.012
enrichment score
rank
Primary Rel
Primary Dx
Relapse_DOWN
NES = -2.213
FDR = 0.012
D
PDX11
PDX30
PDX42
PDX43
OLIGO FCCP ROT/AA
OCR (pmoles/min)
Minutes
Maximal
Basal
Dx
Rel
E
Maximal respiration OCR (pmoles/min)
PDX #
11
30
42
43
Dx
Rel
F
PDX42D
PDX43D
OLIGO FCCP ROT/AA
Maximal
Basal
sh TP53 GFP
sh CTL mCherry
G
Maximal respiration OCR (pmoles/min)
PDXD #
30
42
43
ns
sh CTL mCherry
sh TP53 GFP

# Figure 5

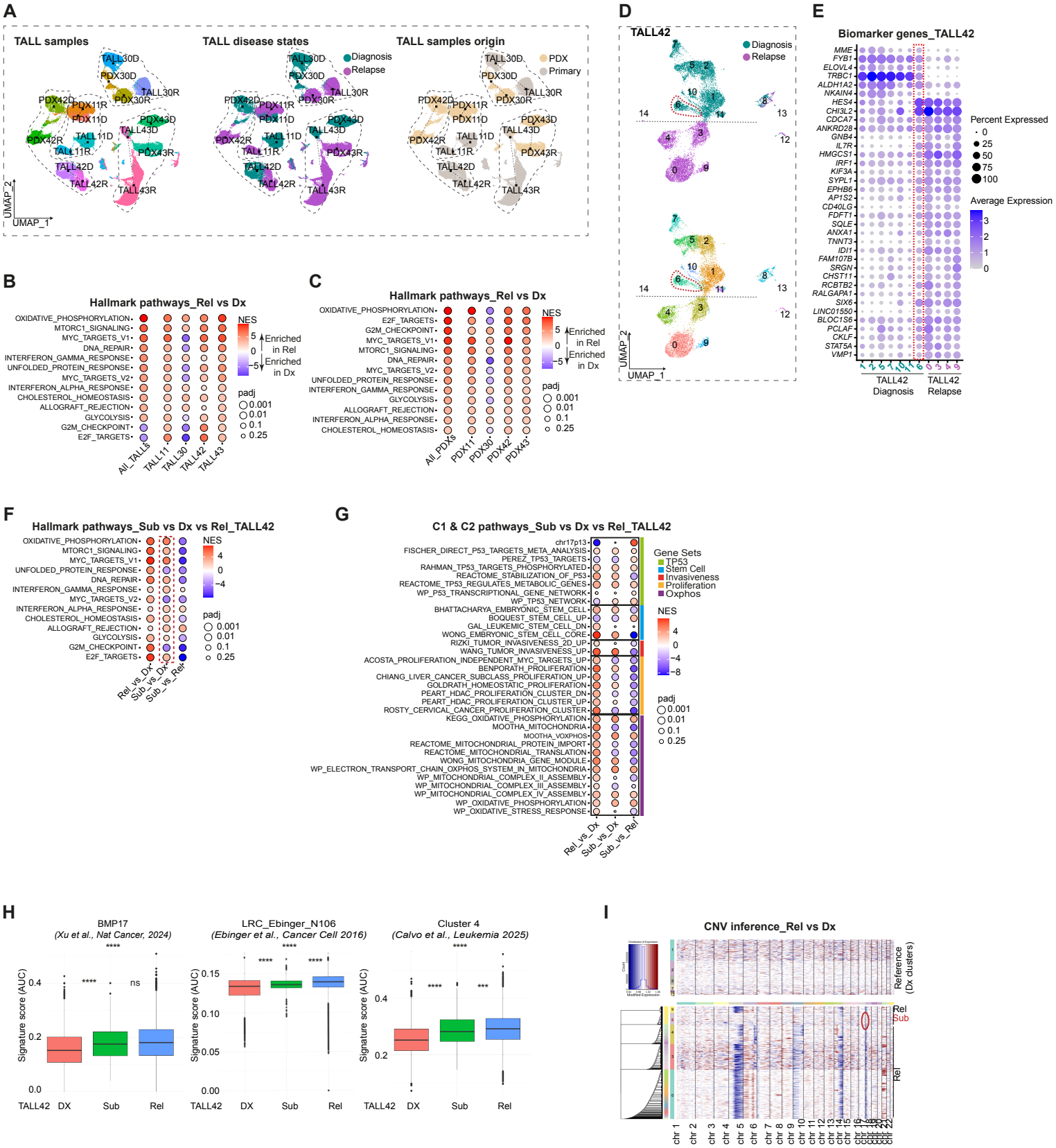
A
TALL samples
TALL disease states
TALL samples origin
Diagnosis
Relapse
PDX
Primary
UMAP_1
UMAP_2
B
Hallmark pathways_Rel vs Dx
NES
Enriched in Rel
Enriched in Dx
padj
C
Hallmark pathways_Rel vs Dx
D
TALL42
E
Biomarker genes_TALL42
Percent Expressed
Average Expression
TALL42 Diagnosis
TALL42 Relapse
F
Hallmark pathways_Sub vs Dx vs Rel_TALL42
G
C1 & C2 pathways_Sub vs Dx vs Rel_TALL42
Gene Sets
TP53
Stem Cell
Invasiveness
Proliferation
Oxphos
H
BMP17
(Xu et al., Nat Cancer, 2024)
LRC_Ebinger_N106
(Ebinger et al., Cancer Cell 2016)
Cluster 4
(Calvo et al., Leukemia 2025)
Signature score (AUC)
I
CNV inference_Rel vs Dx
Reference (Dx clusters)
Rel
Sub